BULLETIN OF THE POLISH ACADEMY OF SCIENCES
TECHNICAL SCIENCES, Vol. 58, No. 4, 2010
DOI: 10.2478/v10175-010-0070-y

VARIA

Combining the principles of variable structure, direct torque control, and space vector modulation for induction motor fed by matrix converter

W. JING-XIN* and J. JIAN-GUO

College of Electrical Engineering, Shanghai Jiao Tong University, Shanghai 200240, China

Abstract. This paper presents a novel direct torque control method for an induction motor fed by a matrix converter using the variable-structure sliding mode scheme with the reaching law, in which combined with the space-vector pulse width modulation to ensure a high-performance operation, both in steady state and under transient conditions. The novel variable-structure controllers are designed to provide the fast and accurate torque and flux control which replace the traditional hysteresis comparators. Some experimental results are shown to prove the accuracy and low-ripple operation of the proposed algorithm.

Key words: direct torque control (DTC), induction motor, variable structure control, matrix converter, reaching law.

1. Introduction

The induction motor (IM) fed by a three-phase matrix converter (shown in Fig. 1) has received considerable interest because of the lack of intermediate dc-link which allows a compact design, the sinusoidal input current and output voltage, the adjustable power factor, and the four-quadrant operation [1–2]. The direct torque control (DTC) scheme has been widely used in induction motor drives which can provide the fast torque response, the simple control scheme without the coordinate transformation, and robustness against motor parameter variations [3–9]. The direct torque control scheme for an induction motor fed by a matrix converter was initially presented in [10]. The generation of the voltage vectors required to implement the DTC of an induction motor fed by a matrix converter with the unity input power factor was allowed. However, the conventional DTC algorithm using hysteresis comparators has some drawbacks: it generates large torque, flux and current ripples especially in a low speed range; the input filters are difficult to design because of the variable switching frequency. There exist several methods which are designed to improve the performance of the classic DTC for a conventional inverter drive system, but there are few methods to improve the performance for the matrix converter drive system [3–20]. The small voltage vectors of matrix converter were used in the direct torque control scheme for matrix converter drives to reduce the electromagnetic torque ripples [21], the torque hysteresis comparator is modified in order to distinguish between large and small torque errors, then a new look-up table for direct torque control using small vectors and large vectors of matrix converter is adopted. However, the direct torque control scheme using small vectors of matrix converter is also based on hysteresis comparators. The linear PI torque and flux control using SVM is investigated by Kyo-Beum Lee [11–12]. The hysteresis comparators of torque and flux are replaced by PI controllers, however, the PI controllers are sensitive to the change of motor parameters, speed and load, and PI controllers have a lag phenomenon in the sinusoid response for certain frequencies [17].

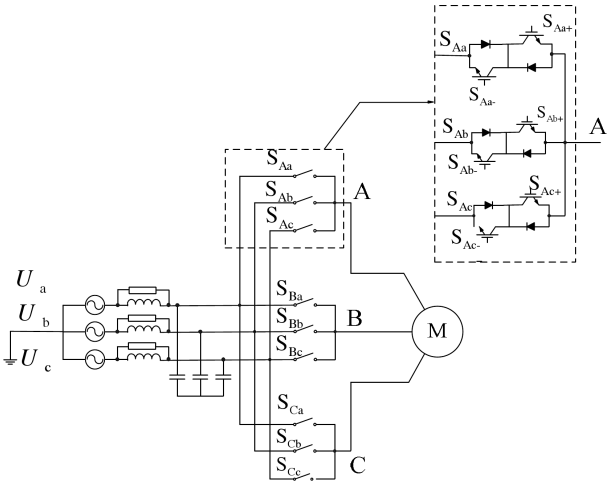

Fig. 1. Schematic representation of matrix converter

The variable-structure control (VSC) is an effective method to overcome these problems. It features robustness to parameter variations of load disturbances, fast dynamic response, and simplicity of design and implementation [15–20]. In this paper, a novel method of the direct torque control using a variable structure control scheme with the space-vector pulsewidth modulation is derived, which is characterized by a constant switching frequency, a fast dynamic torque response and low torque ripples. The effectiveness of the proposed scheme is demonstrated through experimental results.

*e-mail: powerleon82@gmail.com

2. Classic DTC for matrix converter drives

The principle of the classic DTC is based on hysteresis torque and stator flux control that directly selects one of the six nonzero and two zero voltage vectors generated by a conventional two level inverter, in order to maintain the estimated stator flux and torque within the hysteresis bands.

Table 1
Permit switch status list of matrix converter

Switching configuration	Closed switch
+1	$S_{Aa}S_{Bb}S_{Cb}$
-1	$S_{Ab}S_{Ba}S_{Ca}$
+2	$S_{Ab}S_{Bc}S_{Cc}$
-2	$S_{Ac}S_{Bb}S_{Cb}$
+3	$S_{Ac}S_{Ba}S_{Ca}$
-3	$S_{Aa}S_{Bc}S_{Cc}$
+4	$S_{Ab}S_{Ba}S_{Cb}$
-4	$S_{Aa}S_{Bb}S_{Ca}$
+5	$S_{Ac}S_{Bb}S_{Cc}$
-5	$S_{Ab}S_{Bc}S_{Cb}$
+6	$S_{Aa}S_{Bc}S_{Ca}$
-6	$S_{Ac}S_{Ba}S_{Cc}$
+7	$S_{Ab}S_{Bb}S_{Ca}$
-7	$S_{Aa}S_{Ba}S_{Cb}$
+8	$S_{Ac}S_{Bc}S_{Cb}$
-8	$S_{Ab}S_{Bb}S_{Cc}$
+9	$S_{Aa}S_{Ba}S_{Cc}$
-9	$S_{Ac}S_{Bc}S_{Ca}$
0_1	$S_{Aa}S_{Ba}S_{Ca}$
0_2	$S_{Ab}S_{Bb}S_{Cb}$
0_3	$S_{Ac}S_{Bc}S_{Cc}$

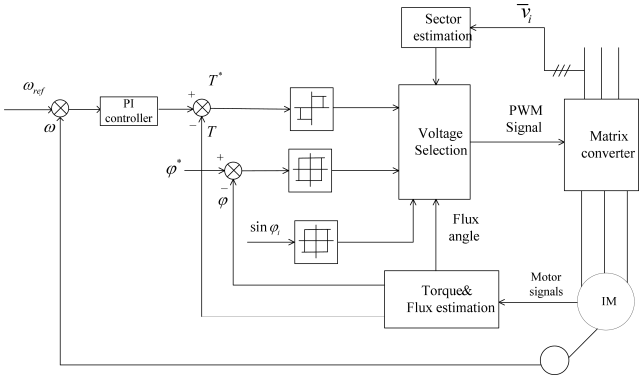

Fig. 2. Block diagram of the DTC scheme with matrix converter

There are 21 possible switching configurations of matrix converter which can be used in DTC algorithm, these configurations are summarized in Table 1. From Table 1, it appears that the matrix converter can generate a higher number of output voltage vectors with respect to two-level inverter. So, DTC for matrix converter drives can control a further variable in addition to stator flux and torque. In [10], the average value of the sine of the displacement angle φ_i between the input line-to-neutral voltage vector and the corresponding input line current vector has been chosen as a third variable. The schematic diagram of DTC for matrix converter drives is represented in Fig. 2. The outer loop contains a speed PI controller which generates the torque reference value for the torque controller, then the reference value of the torque and the stator flux magnitude are compared with the estimated values, the outputs of three hysteresis comparators generate the proper voltage vector with voltage selection policy to restrict the torque, stator flux and the average value of the sine of the displacement angle φ_i within their respective hysteresis bands.

3. Modelling of induction motors

The circuit equations of induction motor in the synchronous speed rotating coordinate are given by (1)

$$\begin{cases} u_{sd} = R_s i_{sd} + \dfrac{d\varphi_{sd}}{dt} - \omega_1 \varphi_{sq} \\ u_{sq} = R_s i_{sq} + \dfrac{d\varphi_{sq}}{dt} + \omega_1 \varphi_{sd} \\ 0 = R_r i_{rd} + \dfrac{d\varphi_{rd}}{dt} - (\omega_1 - \omega)\varphi_{rq} \\ 0 = R_r i_{rq} + \dfrac{d\varphi_{rq}}{dt} + (\omega_1 - \omega)\varphi_{rd} \end{cases}, \tag{1}$$

where u_{sd}, u_{sq}, i_{sd}, i_{sq}, φ_{sd}, φ_{sq} are stator voltages, currents and flux linkages in the synchronous speed rotating frame, i_{rd}, i_{rq}, φ_{rd}, φ_{rq} are rotor currents and flux linkages in the synchronous speed rotating frame, R_s is stator resistance, R_r is rotor resistance, ω_1 is synchronous angular velocity, ω is rotor electrical speed.

The flux linkages equations of induction motor are given by (2)

$$\begin{cases} \varphi_{sd} = L_s i_{sd} + L_m i_{rd} \\ \varphi_{sq} = L_s i_{sq} + L_m i_{rq} \\ \varphi_{rd} = L_m i_{sd} + L_r i_{rd} \\ \varphi_{sd} = L_m i_{sq} + L_r i_{rq} \end{cases}, \tag{2}$$

where L_s is stator self-inductance, L_r is rotor self-inductance, L_m is mutual inductance. Using stator currents as the state variables, the induction motor can be modelled by the following equation from (1) and (2)

$$\begin{cases} \dfrac{di_{sd}}{dt} = \dfrac{L_m}{\sigma L_s T_r}\varphi_{sd} + \dfrac{L_m}{\sigma L_s}\omega\varphi_{sq} - \\ \qquad -\dfrac{R_s L_r + R_r L_s}{\sigma L_s L_r} i_{sd} + (\omega_1 - \omega) i_{sq} + \dfrac{u_{sd}}{\sigma L_s}, \\ \dfrac{di_{sq}}{dt} = \dfrac{L_m}{\sigma L_s T_r}\varphi_{sq} - \dfrac{L_m}{\sigma L_s}\omega\varphi_{sd} - \\ \qquad -\dfrac{R_s L_r + R_r L_s}{\sigma L_s L_r} i_{sq} - (\omega_1 - \omega) i_{sd} + \dfrac{u_{sq}}{\sigma L_s}, \end{cases} \tag{3}$$

where $\sigma = 1 - L_m^2/L_s L_r$ is leakage coefficient, $T_r = L_r/R_r$ is the rotor time constant.

Equation (3) can be transformed into the stationary reference frame by using (4)

$$\begin{bmatrix} f_\alpha \\ f_\beta \end{bmatrix} = \begin{bmatrix} \cos\theta_s & -\sin\theta_s \\ \sin\theta_s & \cos\theta_s \end{bmatrix} \begin{bmatrix} f_d \\ f_q \end{bmatrix} \tag{4}$$

where θ_s is the angle between the d-axis and α-axis.

And the model of the induction motor can be described by (5)–(8)

$$\begin{cases} \dfrac{di_{s\alpha}}{dt} = \dfrac{1}{\sigma L_s T_r}\varphi_{s\alpha} + \dfrac{1}{\sigma L_s}\omega\varphi_{s\beta} - \\ \qquad -\dfrac{R_s L_r + R_r L_s}{\sigma L_s L_r} i_{s\alpha} - \omega i_{s\beta} + \dfrac{u_\alpha}{\sigma L_s} \\ \dfrac{di_{s\beta}}{dt} = \dfrac{1}{\sigma L_s T_r}\varphi_{s\beta} - \dfrac{1}{\sigma L_s}\omega\varphi_{s\alpha} - \\ \qquad -\dfrac{R_s L_r + R_r L_s}{\sigma L_s L_r} i_{s\beta} + \omega i_{s\alpha} + \dfrac{u_\beta}{\sigma L_s} \end{cases} \tag{5}$$

$$\begin{cases} \dfrac{d\varphi_{s\alpha}}{dt} = u_\alpha - R_s i_{s\alpha}, \\ \dfrac{d\varphi_{s\beta}}{dt} = u_\beta - R_s i_{s\beta}, \end{cases} \tag{6}$$

where u_α, u_β, $i_{s\alpha}$, $i_{s\beta}$, $\varphi_{s\alpha}$ and $\varphi_{s\beta}$ are stator voltages, currents and flux linkages in the stationary reference frame.

$$T = \frac{3}{2}P(\varphi_{s\alpha} i_{s\beta} - \varphi_{s\beta} i_{s\alpha}) \tag{7}$$

where T is the estimated torque and P is the number of pole pairs

$$\varphi = \varphi_{s\alpha}^2 + \varphi_{s\beta}^2, \tag{8}$$

where φ is the square of stator flux linkage.

4. Variable structure control scheme

The variable structure control strategy is based on the design of discontinuous control signal that drives the system states towards special manifolds in the state-space [16–19]. There are many different ways to control the parameters of each structure and to define the switching logic [15–20]. In this paper, the strategy is based on torque and square of stator flux variable structure controllers, the block diagram of the proposed strategy is shown in Fig. 3. The outer PI controller and the square of the stator flux generator produce the reference values of torque and square of stator flux, then the difference between torque and square of stator flux reference values and estimated values are sent to the variable structure direct torque controller, the results of the controller are the control voltage vectors in the stationary frame.

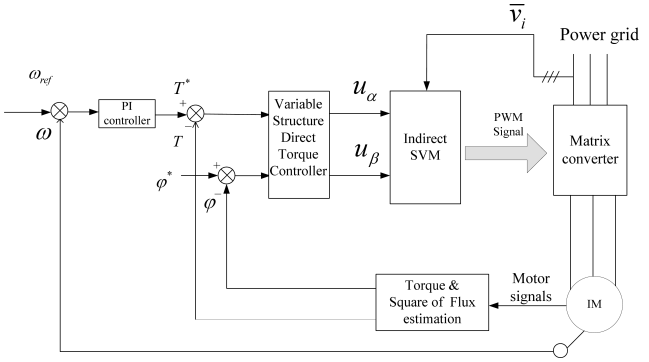

Fig. 3. DTC of induction motor driven by Matrix converter based on variable structure control

4.1. Sliding surfaces. The sliding surface S is designed so as to enforce the sliding-mode operation, we can define up to two switching functions, the sliding surface is set as $S = [S_1 \quad S_2]^T$.

$$\begin{cases} S_1 = \varepsilon_T(t) + K_T \int \varepsilon_T(\tau)d\tau - \varepsilon_T(0) \\ S_2 = \varepsilon_\varphi(t) + K_\varphi \int \varepsilon_\varphi(\tau)d\tau - \varepsilon_\varphi(0) \end{cases} \tag{9}$$

where $\varepsilon_T = T^* - T$ and $\varepsilon_\varphi = \varphi^* - \varphi$, T^* and φ^* are, respectively, the reference values of torque and square of stator flux, T and φ are estimated torque and square of stator flux. K_T and K_φ are control gains. The first function corresponds to the control law of the electromagnetic torque while the second function defines the control law of the stator flux.

The motion projections of the system on S subspace are derived by differentiating the vector S

$$\begin{cases} \dfrac{dS_1}{dt} = \left(\dfrac{dT^*}{dt} - \dfrac{dT}{dt}\right) + K_T(T^* - T) = -\dfrac{dT}{dt} + K_T\varepsilon_T \\ \dfrac{dS_2}{dt} = \left(\dfrac{d\varphi^*}{dt} - \dfrac{d\varphi}{dt}\right) + K_\varphi(\varphi^* - \varphi) = -\dfrac{d\varphi}{dt} + K_\varphi\varepsilon_\varphi \end{cases} \tag{10}$$

4.2. Variable structure control law. The second stage of the variable structure control law design is to select the stator voltage vector which has to be applied so that the torque and square of stator flux trajectories stay on their sliding surfaces. Substituting for T, φ and their derivatives using (5)–(8) leads to

$$\frac{dS}{dt} = F + DU, \tag{11}$$

where calculation for derivatives of D and F is shown below

$$\begin{cases} F_1 = \dfrac{3}{2}P\left[\dfrac{1}{\sigma L_s}\omega\varphi + \dfrac{R_s L_r + R_r L_s}{\sigma L_s L_r}(\varphi_{s\alpha} i_{s\beta} - \varphi_{s\beta} i_{s\alpha}) - \right. \\ \qquad\qquad \left. -\omega(i_{s\alpha}\varphi_{s\alpha} + i_{s\beta}\varphi_{s\beta})\right] + K_T\varepsilon_T, \\ F_2 = 2R_s\varphi_{s\alpha} i_{s\alpha} + 2R_s\varphi_{s\beta} i_{s\beta} + K_\varphi\varepsilon_\varphi, \end{cases} \tag{12}$$

$$D = -\begin{bmatrix} \dfrac{3}{2}P\left(i_{s\beta} - \dfrac{1}{\sigma L_s}\varphi_{s\beta}\right) & \dfrac{3}{2}P\left(\dfrac{1}{\sigma L_s}\varphi_{s\alpha} - i_{s\alpha}\right) \\ 2\varphi_{s\alpha} & 2\varphi_{s\beta} \end{bmatrix} \tag{13}$$

and $U = [u_\alpha \quad u_\beta]^T$.

In this paper, the time-derivative terms of the system states are designed according to "reaching law". The "reaching law" is a differential equation which specifies the dynamics of a system states [20]. The form of the "reaching law" used is

$$\begin{cases} \dfrac{dS_1}{dt} = -k_1 |S_1|^{\varepsilon_1} \operatorname{sgn} S_1 \\ \dfrac{dS_2}{dt} = -k_2 |S_2|^{\varepsilon_2} \operatorname{sgn} S_2 \end{cases}, \tag{14}$$

$$k_1 > 0, \quad k_2 > 0, \quad 0 < \varepsilon_1 < 1, \quad 0 < \varepsilon_2 < 1,$$

where k_1, k_2, ε_1 and ε_2 are control gains, $\operatorname{sgn} S_1$ and $\operatorname{sgn} S_2$ are sign functions. It can be seen from Eq. (14) that the "reach-

ing law" forces the system state to reach the sliding surface at a variable speed, the convergence rate is faster when the system states are far away from the sliding surface (the values of $|S_1|$ and $|S_2|$ are large), while the convergence rate is slow when the system states are close to the sliding surface (the values of $|S_1|$ and $|S_2|$ are small), so the merits of high-rate convergence and low chattering can be achieved by using this reaching law.

Substituting (14) in (11) leads to

$$U = -D^{-1}\begin{bmatrix} F_1 + k_1 |S_1|^{\varepsilon_1} \operatorname{sgn} S_1 \\ F_2 + k_2 |S_2|^{\varepsilon_2} \operatorname{sgn} S_2 \end{bmatrix}. \tag{15}$$

The main shortcoming of the variable structure is the existence of high-frequency chattering, the high frequency components of the chattering are undesirable because they may excite un-modeled high frequency system dynamics and even result in unforeseen instability [17]. Using the smooth function instead of the switching function around the sliding surface can alleviate the problem, that is

$$\operatorname{sgn}(S_i) = \frac{S_i}{|S_i| + \delta}, \qquad \delta > 0 \qquad i = 1, 2. \tag{16}$$

In order to prove the stability of variable structure control system, the control system should satisfy the Lyapunov stability theory, the Lyapunov function is selected as

$$V = \frac{1}{2} S^T S. \tag{17}$$

The time derivative of V on the state trajectories is given by

$$\frac{dV}{dt} = S^T \frac{dS}{dt}. \tag{18}$$

The time derivative of V on the state trajectories can be written by the following equation with Eq. (14) and (18)

$$\frac{dV}{dt} = -S_1(k_1 |S_1|^{\varepsilon_1})\operatorname{sgn} S_1 - S_2(k_2 |S_2|^{\varepsilon_2})\operatorname{sgn} S_2. \tag{19}$$

It can be seen from Eq. (19) that $\dfrac{dV}{dt} < 0$, hence, the variable structure control system is stable according to the Lyapunov stability theory [17].

5. Double space-vector pulsewidth modulation for matrix converter

A brief introduction of the double space-vector pulsewidth modulation for matrix converter is presented in this section. The double space-vector pulsewidth modulation for matrix converter is fully discussed in [2].

The double space-vector pulsewidth modulation algorithm for a matrix converter has the capability to achieve the full control of both the output voltage vector and the input current vector. Figure 4 shows the synthesis schematic of output voltage vector and input current vector of matrix converter, Fig. 5(a) and (b) show the output voltage vector $\overline{v}_o$ and input current vector $\overline{i}_i$ which have fixed directions but variable magnitudes depend upon the instantaneous values of the input line-to-line voltages and output line currents, respectively.

The SVM algorithm is based on the selection of four active vectors which are listed in Table 2 and zero vectors that are applied for the whole cycle period. The duty cycles of the 4 active vectors can be calculated as follows with the absolute values [2]

$$\delta_1 = (-1)^{k_v+k_i} \frac{2}{\sqrt{3}} m \frac{\cos(\theta_o - \pi/3)\cos(\theta_i - \pi/3)}{\cos\varphi_i}, \tag{20}$$

$$\delta_2 = (-1)^{k_v+k_i+1} \frac{2}{\sqrt{3}} m \frac{\cos(\theta_o - \pi/3)\cos(\theta_i + \pi/3)}{\cos\varphi_i}, \tag{21}$$

$$\delta_3 = (-1)^{k_v+k_i+1} \frac{2}{\sqrt{3}} m \frac{\cos(\theta_o + \pi/3)\cos(\theta_i - \pi/3)}{\cos\varphi_i}, \tag{22}$$

$$\delta_4 = (-1)^{k_v+k_i} \frac{2}{\sqrt{3}} m \frac{\cos(\theta_o + \pi/3)\cos(\theta_i + \pi/3)}{\cos\varphi_i}, \tag{23}$$

where θ_o is the output voltage vector angle, θ_i is the input current vector angle, and φ_i is the input displacement angle, m is the voltage transfer ratio, k_v is the sector number of output voltage vector, k_i is the sector number of input current vector, the duty cycle for the zero vector is

$$\delta_0 = 1 - (\delta_1 + \delta_2 + \delta_3 + \delta_4). \tag{24}$$

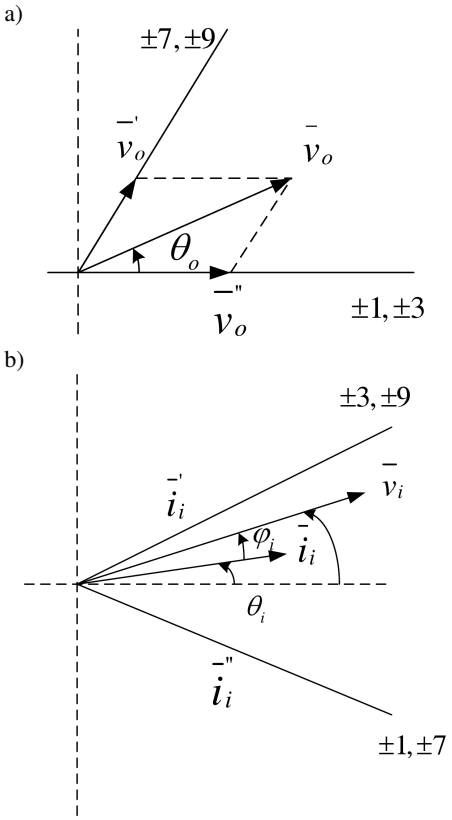

Fig. 4. Synthesis schematic of output voltage vector and input current vector: a) synthesis of output voltage vector b) synthesis input current vector

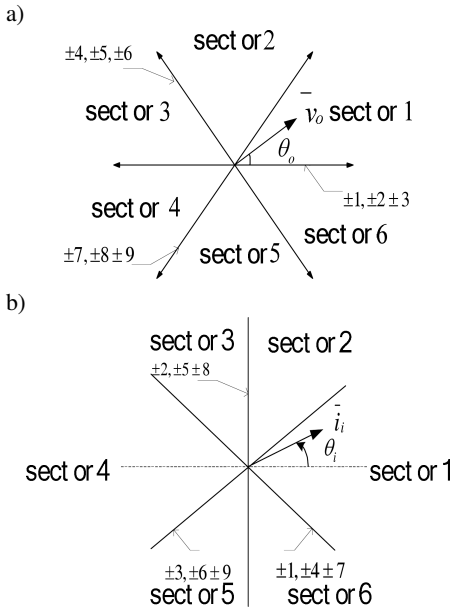

Fig. 5. Sector diagram of output voltage vector and input current vector: a) output voltage vector sector b) input current vector sector

Table 2
Switch status selection of matrix converter

Input current	0utput voltage											
	1 or 4				2 or 5				3 or 6			
1 or 4	9	7	3	1	6	4	9	7	3	1	6	4
2 or 5	8	9	2	3	5	6	8	9	2	3	5	6
3 or 6	7	8	1	2	4	5	7	8	1	2	4	5
status	I	II	III	IV	I	II	III	IV	I	II	III	IV

It should be noted that two of the values calculated by (20)–(23) must be negative values, the negative value of the duty cycle means that the corresponding negative switching configuration has to be selected instead of the positive one. It can be seen from Table 2 that the switching status selection of matrix converter is 9, 7, 3 and 1 when $k_v = 1$ and $k_i = 1$, the values of δ_1 and δ_4 are positive while the values of δ_2 and δ_3 are negative calculated by (20)–(23), so the final switching status selection is $+9$, -7, -3 and $+1$ which can be seen in Table 1.

6. Experiments

Experiments are carried out to confirm the validity of the proposed scheme. The experimental setup of the proposed control system, shown in Fig. 6, consists of three-phase, 380 V, 50 Hz, 5.5 kW induction motor, control system using DSP (TMS320F2812) and FPGA (XC3S50AN-TQ144) with a 12-bit A/D converter board, in which the DSP and A/D converter board completed the variable structure control algorithm, and the FPGA completed the four-step communication and pulses generation for matrix converter. The induction motor has the following parameter values: $R_s = 1.517\ \Omega$, $R_r = 1.483\ \Omega$, $L_s = 0.174$ H, $L_r = 0.174$ H, $L_m = 0.1928$ H. The parameter values of variable structure control system are: $k_1 = 9000$, $k_2 = 9000$, $\varepsilon_1 = 0.5$, $\varepsilon_2 = 0.5$, $\delta = 0.3$, $K_T = 3.0$, $K_\varphi = 4.0$. In order to compare the performance between the classic DTC and proposed DTC, the sampling period is 90 μs for the classic hysteresis band-based DTC, the average switching frequency of classic hysteresis band-based DTC drives is 1.3 kHz, and the sampling frequency is also 1.3 kHz for proposed DTC using space vector modulation.

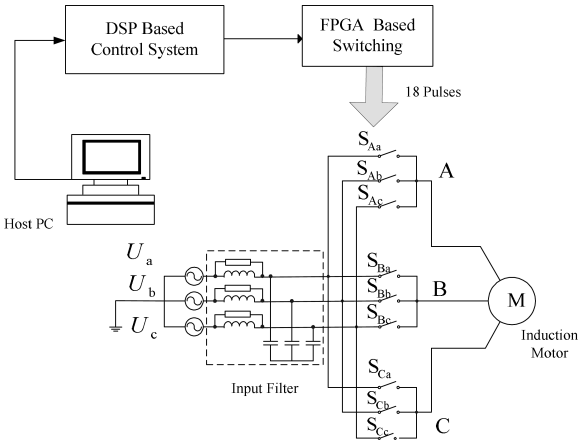

Fig. 6. Experimental system

Figure 7 shows the estimated results of the steady state performance of the classic DTC at 500 rpm, Fig. 8 shows the estimated results of the steady state performance of the proposed variable-structure controlled DTC at 500 rpm. It can be seen from the results that the torque ripples are significantly reduced by the proposed algorithm. Figure 9 shows the estimated result of torque response from 15 Nm∼-20 Nm, it can be seen that the torque response time of the proposed DTC is less than 1ms, which is almost the same as that of the classic DTC. Figure 10 shows the transient performance in a speed reversal process between the values ±500 rpm.

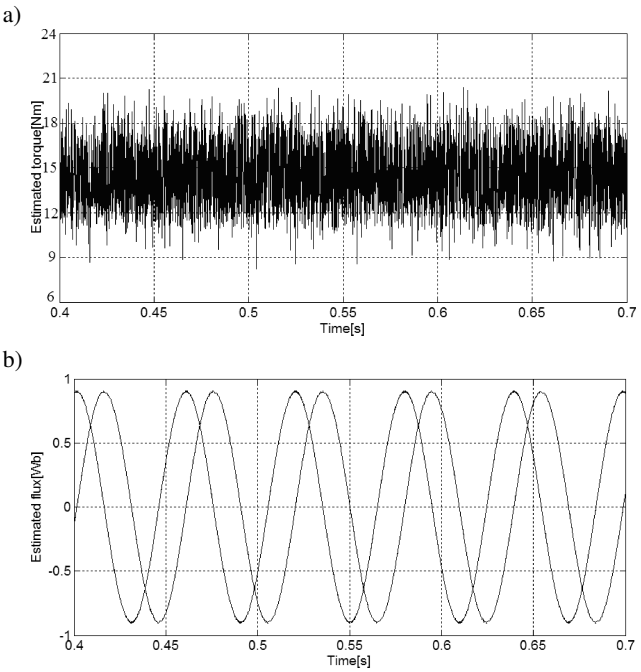

Fig. 7. Estimated steady torque and flux at 500 rpm of classic DTC, $T_s = 90\ \mu s$, a) estimated torque, b) estimated flux

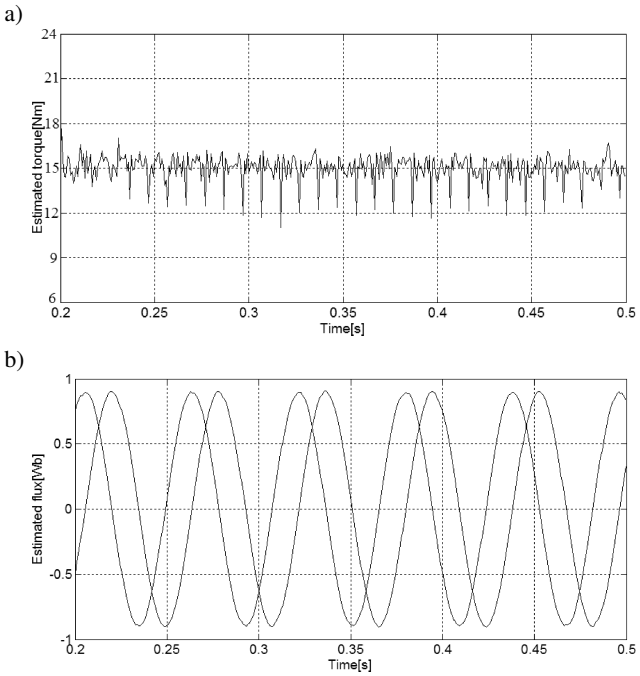

Fig. 8. Estimated steady torque and flux at 500 rpm of proposed DTC, $T_s = 770\ \mu s$, a) estimated torque, b) estimated flux

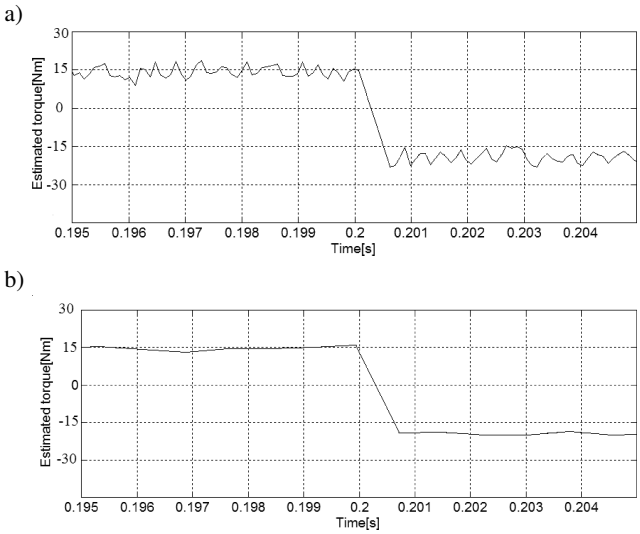

Fig. 9. Torque response from 15 Nm∼-20 Nm, a) torque response of classic DTC, $T_s = 90\ \mu s$, b) torque response of proposed DTC, $T_s = 770\ \mu s$

The response to a speed command and phase current show the good dynamic behaviour. Figure 11 shows the experimental results of the response to a step load from 0 Nm to 15 Nm, once the step change on load torque has been applied, the motor speed is effected by the step load, then the outer speed controller raises the torque demand in order to keep track of speed reference value, it can be seen from Fig. 11 that the motor speed is compensated after 15 ms. Figure 12 shows an input phase source voltage and input current, the line current is in phase with the input phase voltage which allows unity input power factor operation. Figure 13 shows the output line voltage waveform at 900 rpm. The sampling time for Figs. 10–13 is 150 μs.

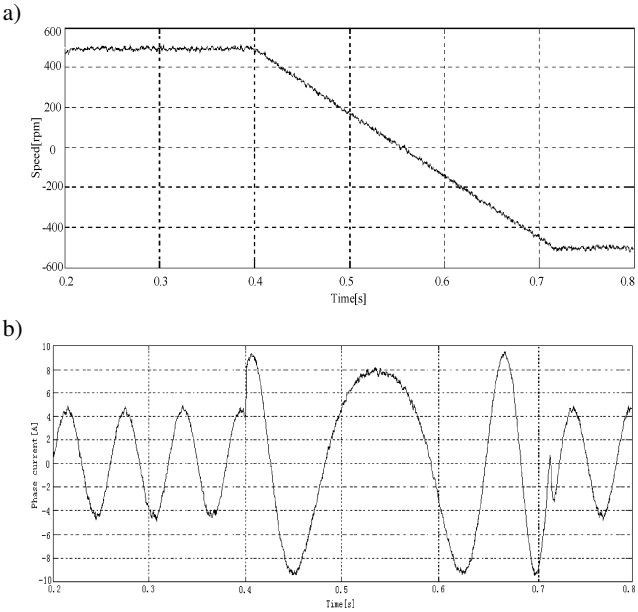

Fig. 10. Speed and current response from +500 rpm∼-500 rpm, $T_s = 150\ \mu s$, a) speed response, b) motor phase current response

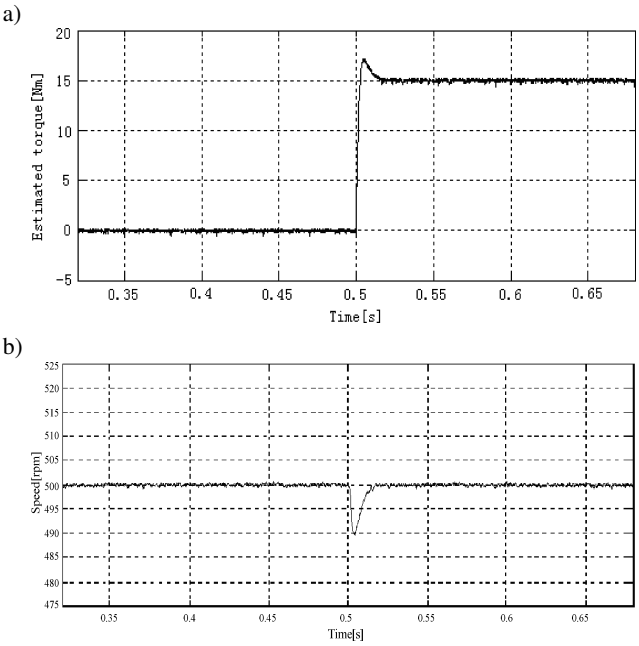

Fig. 11. Experimental results of the response to the step load, $T_s = 150\ \mu s$, a) torque response to the step load, b) speed response to the step load

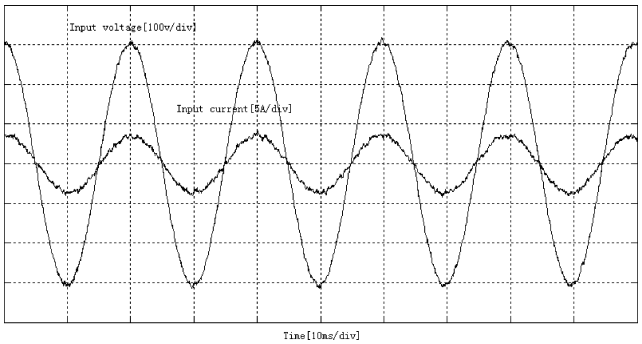

Fig. 12. Input phase voltage and current waveforms, $T_s = 150\ \mu s$

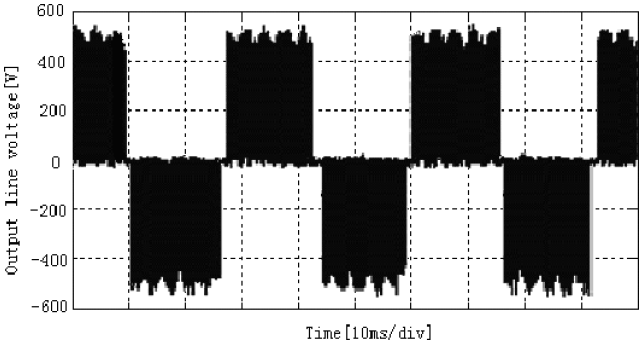

Fig. 13. Output line voltage waveform at 900 rpm, $T_s = 150\ \mu s$

7. Conclusions

In this paper, the variable-structure direct torque control for induction motor fed by a matrix converter has been analyzed. An experimental system composed of an induction motor, a matrix converter and DSP with FPGA control board has been used to validate the proposed algorithm. The performance of the proposed algorithm is improved so that the torque ripples are reduced significantly in comparison with the classic DTC, and also the transient torque response time is almost the same as that of the classic DTC.

REFERENCES

[1] L. Huber and D. Borojevic, "Space vector modulated three-phase to three-phase matrix converter with input power factor correction", *IEEE Trans on Industry Applications* 31 (6), 1234–1246 (1995).

[2] D. Casadei and S. Giovanni, "Matrix converter modulation strategies: a new general approach based on space-vector representation of the switch state", *IEEE Trans. on Industry Electronics* 49 (2), 370–381 (2002).

[3] L. Joong-Hui, K. Chang-Gyun, and Y. Myung-Joong, "A dead-beat type digital controller for the direct torque control of an induction motor", *IEEE Trans. Power Electron.* 17 (5), 739–746 (2002).

[4] L. Yen-Shin and Ch. Jian-Ho, "A new approach to direct torque control of induction motor drives for constant inverter switching frequency and torque ripple reduction", *IEEE Trans. on Energy Convers.* 16 (3), 220–227 (2001).

[5] N.R.N. Idris and A.H.M. Yatim, "Direct torque control of induction machines with constant switching frequency and reduced torque ripple", *IEEE Trans. on Industry Electronics* 51 (4), 758–767 (2004).

[6] R. Ortega, N. Barabanov, and G.E. Valderrama, "Direct torque control of induction motors: stability analysis and performance improvement", *IEEE Trans. on Automatic Control*. 46 (8), 1209–1222 (2001).

[7] N.R.N. Idris, Ch.L. Toh, and M.E. Elbuluk, "A new torque and flux controller for direct torque control of induction machines", *IEEE Trans. on Industry Applications* 42 (6), 1358–1366 (2006).

[8] L. Romeral, A. Arias, E. Aldabas, and M.G. Jayne, "Novel direct torque control (DTC) scheme with fuzzy adaptive torque-ripple reduction", *IEEE Trans. on Industry Electronics* 50 (3), 487–492 (2003).

[9] Y.-S. Lai, W.-K. Wang, and Y.-C. Chen, "Novel switching techniques for reducing the speed ripple of AC drives with direct torque control", *IEEE Trans. on Industry Electronics* 51 (4), 768–775 (2004).

[10] D. Casadei and S. Giovanni, "The use of matrix converter in direct torque control of induction machines", *IEEE Trans. on Industry Electronics* 48 (6), 1057–1064 (2001).

[11] K.-B. Lee and F. Blaabjerg, "An improved DTC-SVM method for sensorless matrix converter drives using an overmodulation strategy and a simple nonlinearity compensation", *IEEE Trans. on Industry Electronics* 54 (6), 3155–3166 (2007).

[12] K.-B. Lee and F. Blaabjerg, "Sensorless DTC-SVM for induction motor driven by a matrix converter using a parameter estimation strategy", *IEEE Trans. on Industry Electronics* 55 (2), 512–521 (2008).

[13] K.-B. Lee and F. Blaabjerg, "Improved sensorless vector control for induction motor drives fed by a matrix converter using nonlinear modeling and disturbance observer", *IEEE Trans. on Energy Convers.* 21 (1), 52–59 (2006).

[14] G.S. Buja and M.P. Kazmierkowski, "Direct torque control of PWM inverter-fed ac motors-a survey", *IEEE Trans. on Industry Electronics* 51 (4), 744–757 (2004).

[15] C. Lascu, I. Boldea, and F. Blaabjerg, "Very-low-speed variable-structure control of sensorless induction machine drives without signal injection", *IEEE Trans. on Ind. Appl.* 41 (2), 591–598 (2005).

[16] C. Lascu, I. Boldea, and F. Blaabjerg, "Direct torque control of sensorless induction motor drives: a sliding-mode approach", *IEEE Trans. on Ind. Appl.* 40 (2), 582–590 (2004).

[17] Z. Xu and M. F. Rahman, "Direct torque and flux regulation of an IPM synchronous motor drive using variable structure control approach", *IEEE Trans. on Power Electron.* 22 (6), 2487–2498 (2007).

[18] V.I. Utkin, "Sliding mode control design principles and applications to electric drives", *IEEE Trans. on Ind. Electron.* 40 (1), 23–36 (1993).

[19] C. Lascu and A.M. Traynadlowski, "Combining the principles of sliding mode, direct torque control, and space vector modulation in a high-performance sensorless AC drive," *IEEE Trans. on Ind. Appl.* 40 (1), 170–177 (2004).

[20] A. Naassani, E. Monmasson, and J.P. Louis, "Synthesis of direct torque and rotor flux control algorithms by means of sliding-mode theory", *IEEE Trans. on Ind. Electron.* 52 (3), 785–799 (2005).

[21] C. Ortega, A. Arias, and J. Ballcells, "The use of small voltage vectors of matrix converters in direct torque control of induction machines", EPE-PEMC 1, 314–319 (2006).